Al-Qadisiyah Journal of Pure Science

ISSN(Printed): 1997-2490 ISSN(Online): 2411-3514

DOI: 10.29350/jops

Al-Qadisiyah Journal of Pure Science

Study of Adsorption Kinetics of Copper ions using Activated Charcoal / ZnO as a Binary Nanocompasite

Haider Nazar Hussein[1] Safa Ahmed Yassin[2] and Donia Ahmed Abdulateef [3]

The General Directorate for Education of Diyala,

Corresponding author E-mail: haiderghrabee@gmail.com

Tel: +964 773 352 3063

Abstract: As a binary nanocompasite, studies have been done on the adsorption of copper ions (Cu^{+2}) from an aqueous solution on activated charcoal/ZnO nanoparticles (ZnO/AC). Equilibrium and kinetic isotherms were investigated using batch shaking adsorption experiments. The findings demonstrate that copper ions from an aqueous solution may be successfully removed using activated charcoal. Six isotherm models were used to the experimental data in order to forecast the adsorption isotherms and ascertain the distinctive parameters for process design: Langmuir, Freundlich, Elovich, Temkin, and Henry's. We looked at the equilibrium facts. The results show that Henry's > Freundlich > Temkin > Elovich > Langmuir is the order in which the adsorption isotherm models matched the data. Two models were used to examine the adsorption kinetic data: the pseudo-first order and the pseudo-second order models. According to kinetic investigations, both models were followed in the adsorption of copper ions onto AC, ZnO, and ZnO/AC.

Keywords — activated carbon, ZnO nanoparticles, Copper ions, adsorption isotherms, kinetic models.

INTRODUCTION

The growing demand for products produced by the chemical industry is the cause of the accumulation of heavy metals in the environment [1]. Heavy metal contamination of aquatic media is a severe environmental issue [2]. The main sources of copper ions are industrial wastewater from metal cleaning, plating baths, refineries, paper and pulp, fertilizers, tanneries, and wood preservatives [3]. Elevated copper concentrations cause enzyme inhibition, which is the cause of Wilson's illnesses [4]. An estimated millions grams from toxic metals, such as Pb, Cd, Hg, As, Cu , Al, as well as particulate matter were released into freshwater environments each year by industry, and millions grams of copper were disposed of globally in sewage and industrial waste that ended up in the rivers

[5]. The World Health Organization (WHO) established a maximum of 1.5 parts per million (ppm) of copper in drinking water [6]. Many metal removal techniques used, adsorption techniques have been shown to be a successful and desirable way to remove non-biodegradable contaminants from wastewater [7,8]. The word composite explain the newfound understanding that biological material enhanced by nanomaterial can be used in addition to adsorption to remove particles, chemicals, and metals from solutions [9,10]. Biosorbents include things like activated charcoal [11], biochar and various biopolymers [12]. The second most plentiful organic material on Earth is activated charcoal. It is extensively utilized for the adsorption of heavy metal ions [13]. According to Eduardo and colleagues' findings, ZnO NPs exhibit significant adsorption capabilities and a strong affinity for Cu(II) ions [14]. Investigating the adsorption of copper (II) ions on ZnO / activated charcoal nanocompasite is the goal of this work. Equilibrium data from adsorption are used to analyze the adsorption equilibrium on the nanomaterials synthesized.

MATERIALS ANDMETHODS

Chemicals

Copper chloride was used to prepare a stock solution of copper in deionized water. The stock solution was diluted to prepare all additional solutions. The concentrations of copper ions were measured with an atomic absorption spectrophotometer. $ZnCl_2$ salt using as a source of ZnO nanoparticles.

Preparation of Activated charcoal

The charcoal came from burning the willow stems in the Diyala orchards using crude techniques. The 100 grams of stem willow charcoal were finely ground into a powder. After letting the charcoal powder air dry for a full day, whisk in 50 milliliters of lemon juice to create a cohesive paste. To make activated carbon, or activated charcoal, the mixture was covered, let to sit for a full day, and then baked at 150 ^{o}C for five hours.

Preparation of zinc oxide nanoparticles

(1 g) from zinc (II) chloride ($ZnCl_2$) was dissolved in (100 mL) of deionized water with continuous stirring and then (20 mL) of plant extract is added gradually with continuous stirring at room temperature, raise temperature of solution to (80°C) and then adjusts pH of the solution until pH reached to 12 by adding sodium hydroxide (0.1 M) approximately (20 mL), the precipitate of ($Zn(OH)_2$) was formed after 5 minute, filtered and washed

with deionized water several times and then with absolute ethanol to remove impurities and calcination process of sample in a furnace at (550°C) for (5) hours to obtained zinc oxide nanoparticles (ZnO NPs).

Preparation of zinc oxide / Activated charcoal as a binary nanocomposite

Using impregnation method the ZnO/AC nanocomposite were synthesized (1g AC: 0.5 g nano ZnO). An impregnated solution was prepared by suspended (1g) AC and (0.5 g) ZnO in ethanol (20 mL) at room temperature with constant stirring; the mixture was placed in water Bath apparatus. After 2 hours the nanoparticles are completely suspended and the solvent was evaporated to obtain a ZnO/AC as a binary nanocomposite.

Adsorption Experiments

In various conical flasks, batch adsorption experiments were conducted at room temperature (25°C). Each flask was filled with varying weights of adsorbents (activated charcoal), such as 1, 2, 3, 4, and 5 g. Each flask on the adsorbents received 30 mL of CuCl2 solution added to it. To achieve equilibrium, the mixture was shaken for an hour using a shaker. The solution was then filtered, and an atomic absorption spectrophotometer was used for analysis. The percentage of removed copper ions in solution was calculated using Equation:

$$\%\text{Removed} = \frac{(C_o - Ce)}{C_o} \text{ x } 100$$

The mass balance relationship showed that the amount of copper adsorbed at equilibrium, qe (mg/g), could be computed as follows:

$$qe = \frac{(C_o - Ce) * V}{wt}$$

RESULTS AND DISCUSSION

Figure 1 shows the XRD plots of the ZnO/AC nanocomposite and ZnO nanoparticles that were synthesized. Particle crystalline structure and crystallite size can be inferred from XRD analysis. Figure 1 displays the XRD pattern for the biogenic synthesized ZnO NPs. According to JCPSD card no. 00-230-0450, the hexagonal crystal geometry and the XRD peaks at 2θ = 2θ: 31.7729º, 34.4268º, 36.2585º, 47.5466º, 56.6023º, 62.8681º, 66.3862º, 67.9599º, and 69.0953º correspond to the (100), (002), (101), (102), (210), (103), (200) crystal planes and the hexagonal crystal geometry. The other XRD peaks of the ZnO/AC nanocomposite in Figure 1 can be attributed to the crystallized ZnO NPs. Further, the XRD peak in the case of ZnO/AC nanocomposite confirms ZnO NPs-AC interaction [15]. The average particle size of the ZnO NPs was determined by using the Scherrer equation:

$$D = \frac{K\lambda}{\beta cos\theta}$$

Where D is the size of the crystallite, λ is the x-ray wavelength, k is the form factor or constant, approximately 0.9, β is the entire breadth at the half-maximum of the diffraction peak, and θ is the diffraction angle.

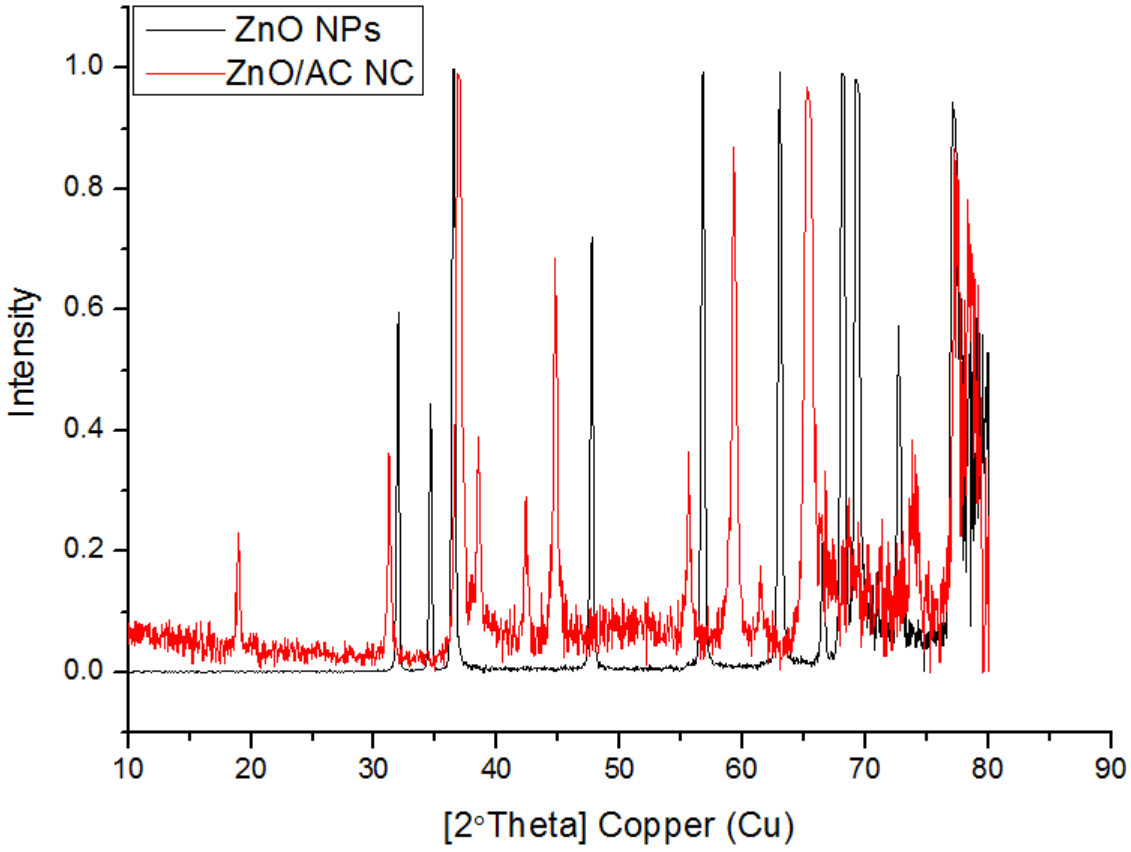

Fig.1. XRD pattern of ZnO NPs and ZnO / AC nanocomposite.

Activated charcoal (AC), ZnO NPs and ZnO/AC nanocomposite adsorbents were examined for surface morphology using FE-SEM analyses, see figures 2 (a through c). The FE-SEM micrograph in Figure 2 (a) show that the surface of the prepared activated charcoal has a variety of irregular pores, including mesopores and micropores. Images of the ZnO NPs surface morphology are shown in figure 2 (b), which scan of the adsorbent surface reveals the presence of 195 nm-diameter, irregularly shaped particle agglomerates. While, figure 2 (c) exhibit the FE-SEM image of ZnO/AC nanocomposite, which show at a magnification of 50 kx clearly show the cloud-like structures with irregular facets and sharp edges between them with structures have an average size of 56.42 nm.

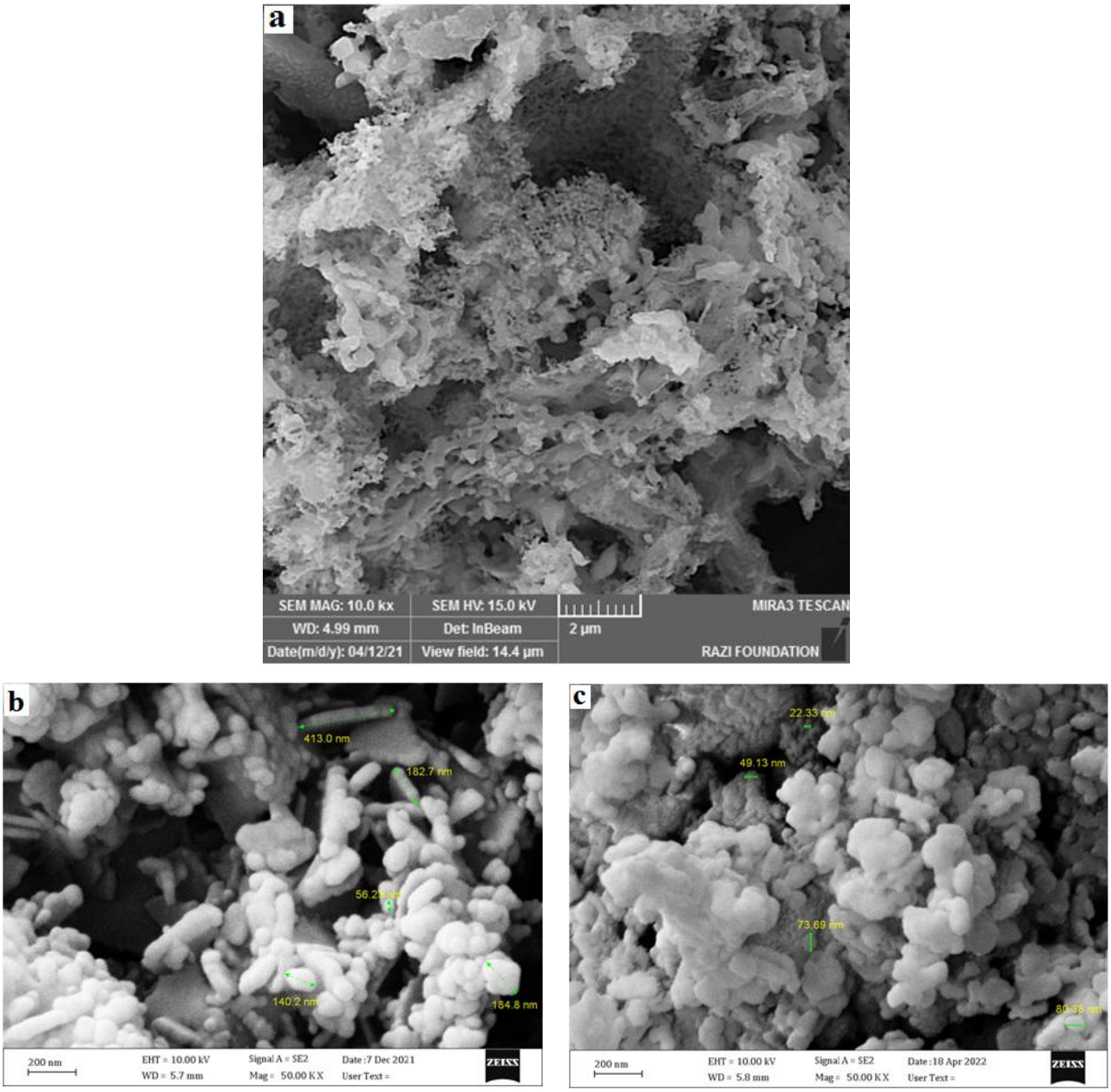

Fig.2. FESEM images of (a) activated charcoal, (b) ZnO nanoparticles, and (c) ZnO/AC nanocomposite's

Figure 3(a and b) displays TEM images of the ZnO nanoparticles and ZnO/AC nanocompasite obtained using a transmission electron microscope. The size of the roughly spherical ZnO nanoparticles and ZnO/AC nanocompasite were approximately 22 nm and 34 to 40.5 nm, respectively.

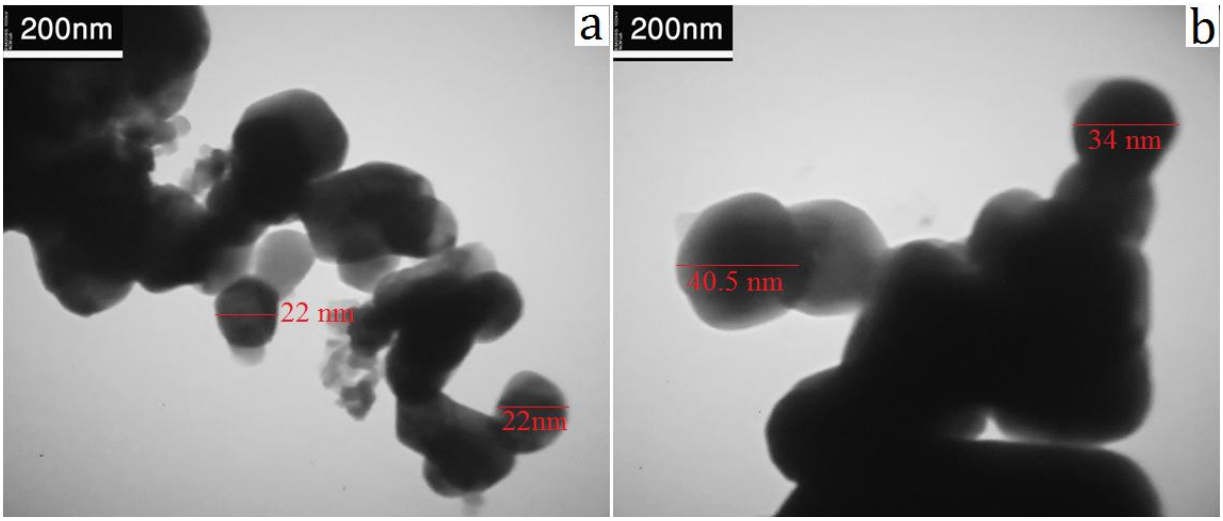

Fig. 3. TEM images of (a) ZnO NPs, and (b) ZnO/AC nanocompasite

Adsorption of Cu(II) ions on nanomaterials

Effect of contact time on adsorption

The investigation looked at the effects of contact time at concentrations of 100 mg/L of copper ions at temperatures of 298 K for 20, 40, 60, 80, 100, and 120 minutes on the adsorption of Cu^{+2} ions on activated charcoal (AC), ZnO nanoparticles, and ZnO/AC. The percentage removal changes as the contact time of Cu^{+2} increases, as shown in Figure 4(a). According to what they have shown, the equilibrium time needed for the adsorption of copper ions on activated charcoal (AC), zinc oxide nanoparticles, and zinc oxide/AC) are almost 100 minutes. During this time, the percentage removal for surfaces decreases at the beginning of the contact time and gradually increases at the end. The adsorbent may have an overabundance of adsorption sites, which might explain this. Ion exchange may have caused the high adsorption rate at first, and the sluggish chemical reaction involving the metal ions' active groups on the sample may have followed. It is challenging to occupy the remaining vacant surface areas due to repulsive force. The metal ions encounter increasing resistance as they pass through the pores, going deeper and farther.

Effect of adsorbent quantity on adsorption

Activated charcoal (AC), ZnO NPs, and ZnO/AC surfaces were used as study materials. Various adsorbent quantities (0.1, 0.2, 0.4, 0.6, 0.8, and 1) g were used at (298) K, using a fixed Cu^{+2} ion concentration of 100 mg/L and a 100-minute contact duration. Figure 4(b) shows how the amount of adsorbent influences the absorption of Cu+2 ions onto ZnO NPs, ZnO/AC, and activated charcoal (AC). A higher quantity of adsorbents results in a higher

percentage removal of copper ions. The increasing surface area explains the increase in the percentage removal.

Effect of temperature on adsorption

The study materials included ZnO NPs, ZnO/AC surfaces, and activated charcoal (AC). The following parameters were used: 1 g of nanomaterials; fixed concentration of Cu^{+2} ions (100 mg/L); contact period (100 minutes); and various adsorbent temperatures (298, 318, 338, 358, 378, and 398 K). The temperature impact, which influences Cu^{+2} ion absorption onto activated charcoal (AC), ZnO NPs, and ZnO/AC, is depicted in Figure 4(c). A higher temperature results in a less percentage of copper ions being removed.

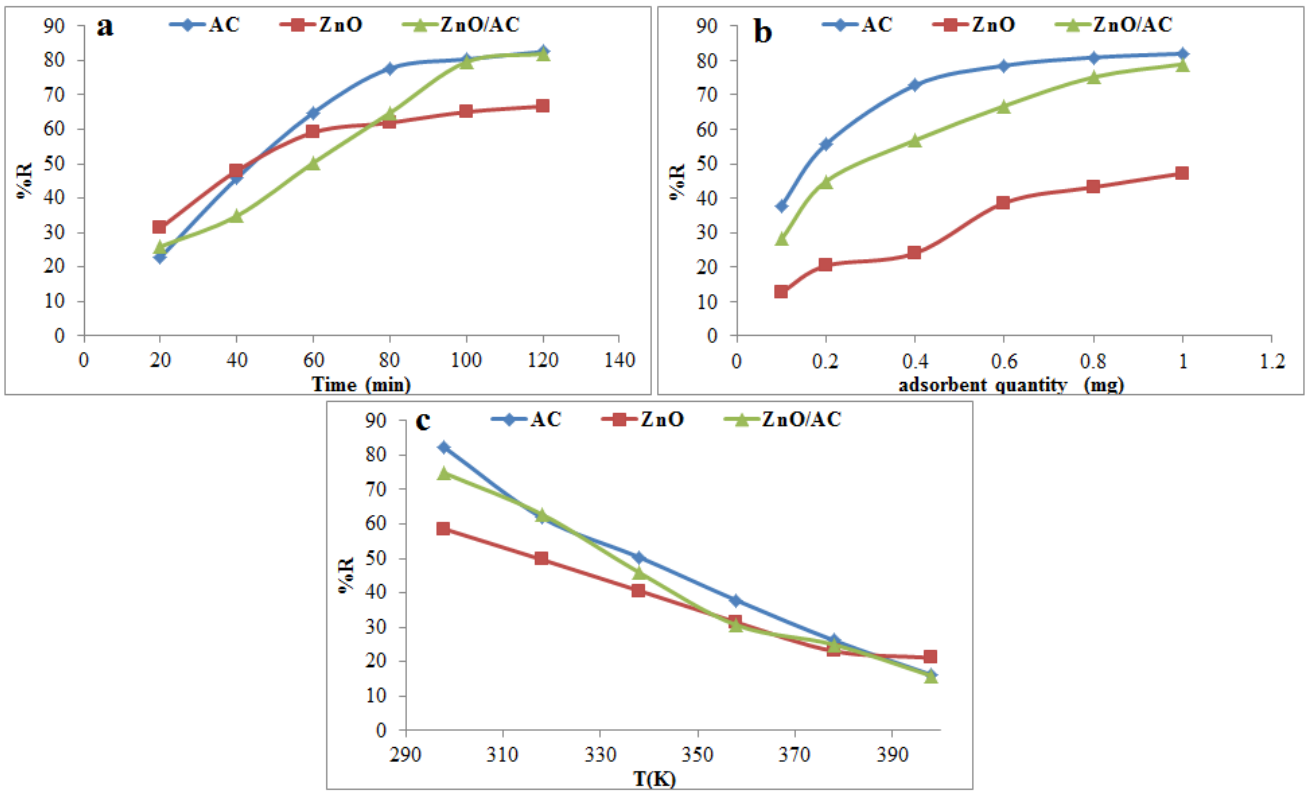

Fig.4. Effect of (a) contact time, (b) adsorbent quantity, and (c) temperature effect of Cu^{+2} removal (%) over Activated charcoal (AC), ZnO NPs and ZnO/AC materials surfaces.

Kinetics Studies of Adsorption Process for Cu^{+2}

Among other kinetic models, pseudo-first- and pseudo-second-order models were tried.

The Pseudo-First-Order Model

One of the rate equations that is most frequently used to explain the adsorption of an adsorbate from the liquid phase is Lagergren's rate equation. The linear form of the pseudo-first-order equation is as follows:

$$ln(\mathrm{qe} - \mathrm{qt}) = lnqe - k1t$$

Figure 5 displays the first order rate constant experimental results. The good regression coefficient of the adsorption data indicates that the pseudo-first order adsorption kinetics may be followed by copper adsorption on the sorbent.

Based on the premise that the rate of change of solute uptake with time is directly proportional to the difference in saturation concentration and the amount of solid uptake with time, the Lagergren pseudo-first-order model is commonly applicable over the initial stage of an adsorption process.

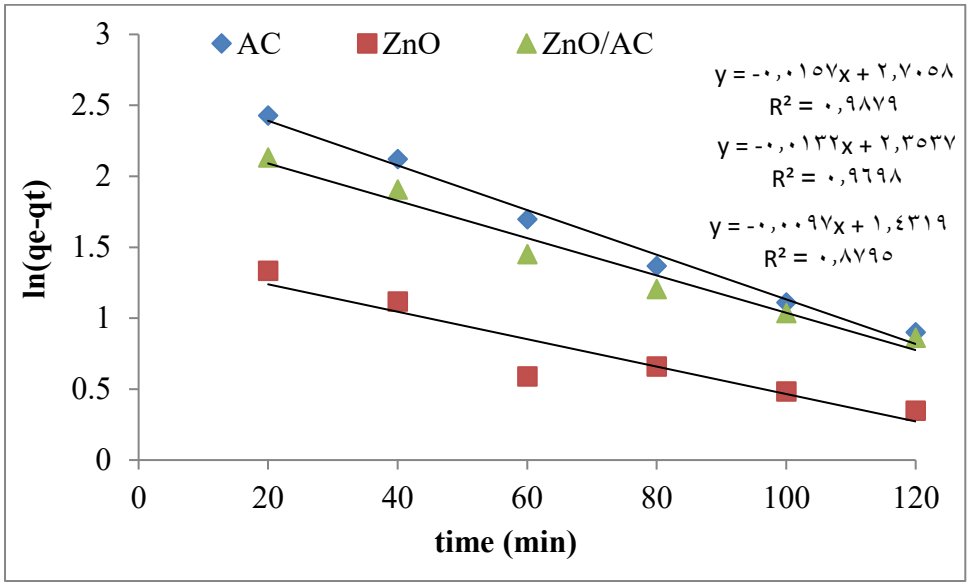

Fig.5. The Pseudo First – Order Kinetic Model for Cu^{+2} ions adsorption on activated charcoal (AC), ZnO NPs and ZnO/AC materials surfaces**.**

The Pseudo-Second-Order model

The pseudo-second order kinetic model is defined as follows and is predicated on the idea that chemisorption is the step that determines rate:

$$\frac{\mathrm{t}}{\mathrm{qt}} = \frac{1}{k2qe2} + \frac{1}{qe}t$$

The acquired data demonstrates a strong agreement with the pseudo-second-order equation. The linear plot's correlation coefficient, R^2, indicates a strong relationship between the parameters and explains how the adsorption process fits into a pseudo-second-order kinetic model (Figure 6).

The pseudo-second-order kinetic model predicts behavior across the complete adsorption range with the assumption that chemical sorption, or chemisorption, is the rate-limiting

phase. In these conditions, the adsorption rate is influenced more by the adsorbate concentration and the adsorption capacity.

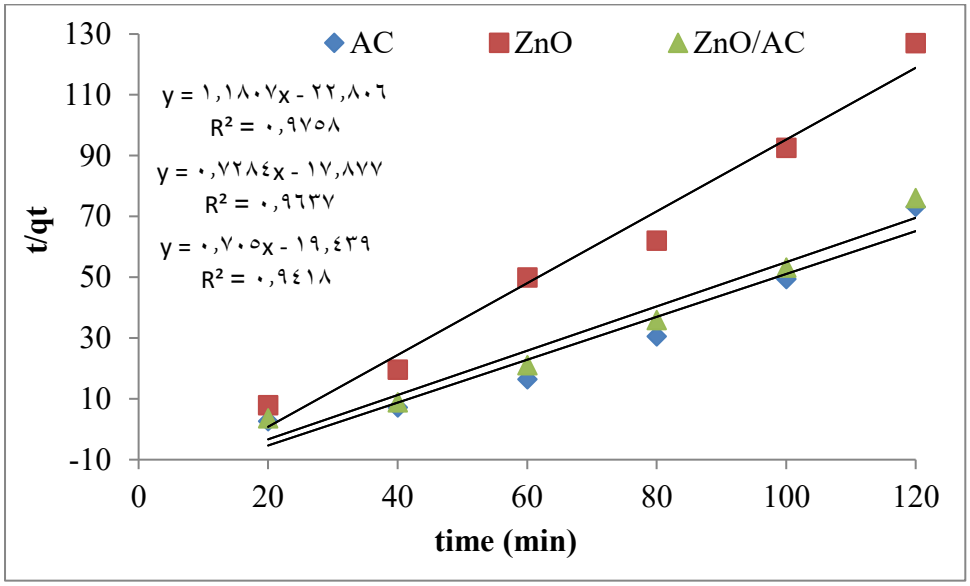

Fig.6. The Pseudo second – Order Kinetic Model for Cu^{+2} ions adsorption on activated charcoal (AC), ZnO NPs and ZnO/AC materials surfaces**.**

Generally speaking, We observe from the above-mentioned kinetic data that the pseudo second order model fits the ZnO/AC sample better than the pseudo first order model. However, depending on the correlation coefficient (R^2), both models fit the activated charcoal sample better than the binary composite and zinc oxide nanoparticles. Table 1 displayed all of the adsorption kinetics constants for the adsorption of Cu^{+2} ions on ZnO NPs, activated charcoal (AC), and ZnO/AC surfaces.

Table 1: Adsorption kinetics constants for Cu^{+2} ions adsorption on activated charcoal (AC), ZnO NPs and ZnO/AC surfaces.

Sample	Pseudo-First-Order			Pseudo-Second-Order		
	qe	K_1	R^2	qe	K_2	R^2
AC	14.96678	0.01573	0.9879	1.418388	-0.02557	0.9758
ZnO	4.18648	0.00966	0.9698	0.846924	-0.03145	0.9637
ZnO/AC	10.52457	0.01316	0.8795	1.372882	-9.48477	0.9418

The adsorption isotherm

Henry's Isotherms.

The amount of surface adsorbate is proportional to the partial pressure of the adsorptive gas in this most basic adsorption isotherm. All adsorbate molecules are kept apart from their closest neighbors when the adsorbate is adsorbed at relatively low concentrations, as described by this isotherm model. The linear expression can be linked to the equilibrium adsorbate concentrations in both the liquid and adsorbed phases.

$$\mathrm{qe} = KHE\ Ce$$

where K_{HE} is Henry's adsorption constant, qe is the amount of adsorbate at equilibrium (mg/g), and Ce is the equilibrium concentration of the adsorbate on the adsorbent.

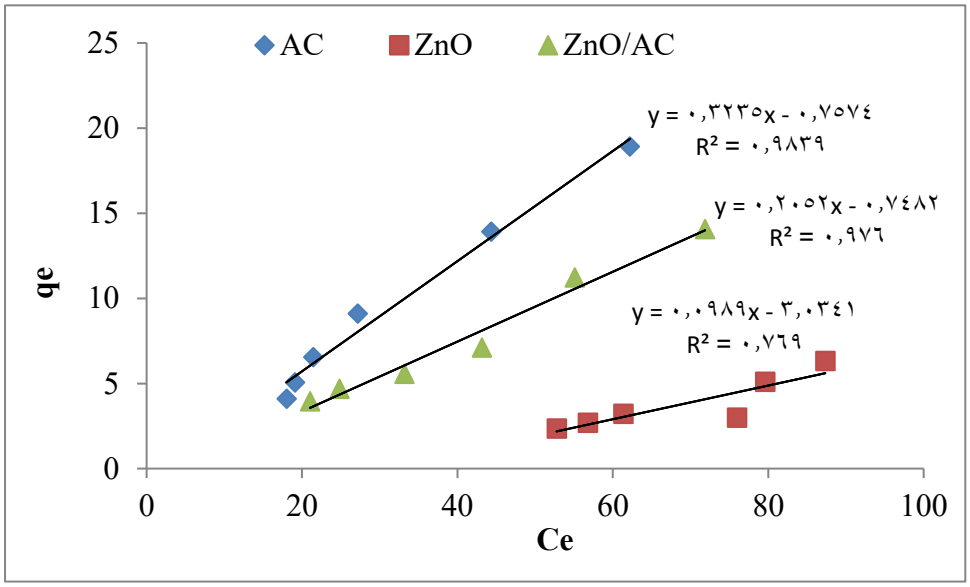

Fig. 7. Henry's adsorption isotherm.

Langmuir Isotherm

Langmuir adsorption, which was initially created to evaluate gas-solid phase adsorption, is used to assess and compare the adsorptive capacities of various adsorbents. The Langmuir isotherm describes the surface coverage by preserving a balance between the relative rates of adsorption and desorption (dynamic equilibrium). The process of adsorption is associated with the exposed portion of the adsorbent surface, whereas the process of desorption is associated with the covered section of the adsorbent surface. The Langmuir equation has the following linear form:

$$\frac{\mathrm{Ce}}{\mathrm{qe}} = \frac{1}{qmke} + \frac{Ce}{qm}$$

where C_adsorbate is the equilibrium concentration (mg g^{-1}). Large surface area and pore volume will lead to larger adsorption capacity, as indicated by the Langmuir constant KL,

which is connected with the variation of the appropriate area and porosity of the adsorbent (mg g^{-1}). A dimensionless constant known as the separation factor R_L can be used to express the fundamental properties of the Langmuir isotherm.

$$RL = \frac{1}{1 + KLC_o}$$

where Co is the initial adsorbate concentration (mg g^{-1}) and K_L is the Langmuir constant (mg g^{-1}). When adsorption is unfavorable, it is indicated by RL values. When adsorption is linear, it is favorable, when $0 < RL < 1$, and it is irreversible when adsorption is favourable.

The correlation coefficient (R^2) from Fig. 7 and are shown in Table 2 show that the dose is not acceptable for the monolayer adsorption fit.

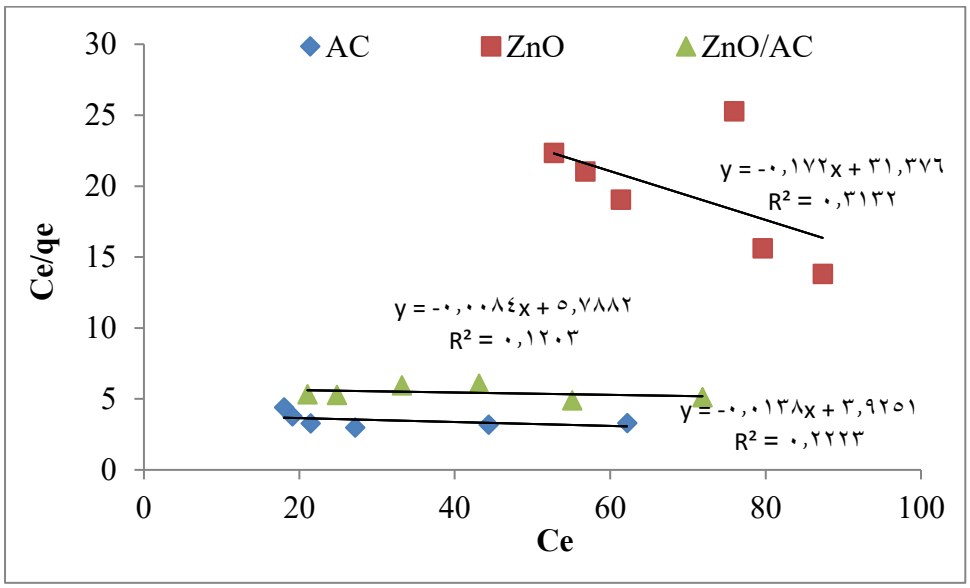

Fig. 7. Langmuir adsorption isotherm.

Freundlich isotherm

The following equation represents the Freundlich sorption isotherm, which provides an expression that includes surface heterogeneity as well as the exponential distribution of active sites and their energies:

$$\log qe = \log kF + \frac{1}{nf} \log Ce$$

Table 2 presents the values of KF and nf, which were determined by calculating the slope and intercept of the linear plot log qe vs log Ce, as illustrated in Figure 8. For AC, ZnO, and ZnO/AC, the correlation coefficient (R^2) values were 0.9733, 0.9614, and 0.7772, respectively. These values are greater than the Langmuir isotherm. Furthermore, a good adsorption is indicated if the value of nf falls between 1 and 10.The values of nf that were

obtained for AC, ZnO, and ZnO/AC were 0.863694, 0.598936, and 0.955096, respectively. suggesting a successful adsorption process.

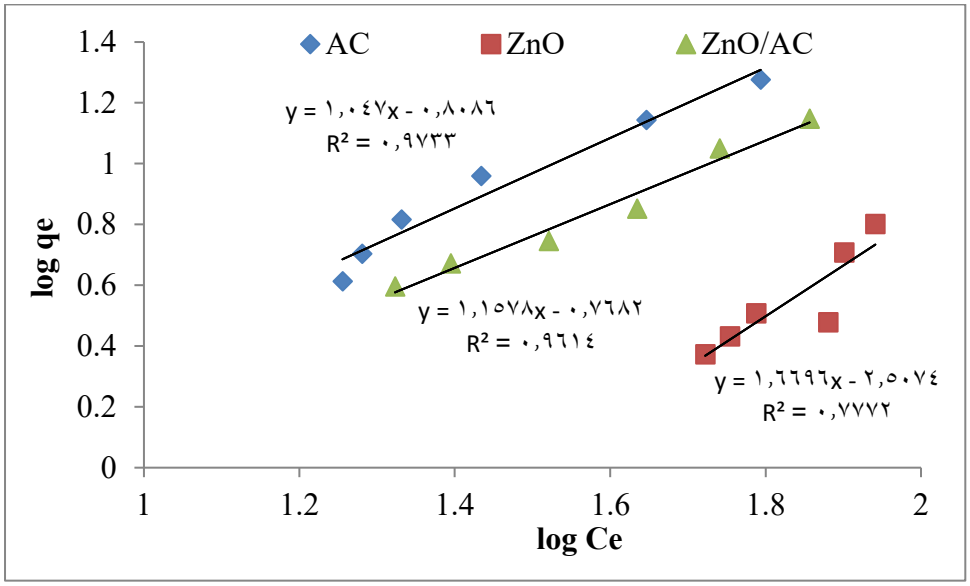

Fig. 8. Freundlich adsorption isotherm.

The Elovich isotherm

A multilayer adsorption is implied by the equation describing the Elovich model, which is based on the kinetic principle and assumes that the adsorption sites expand exponentially with adsorption. It is communicated by the relationship:

$$ln\frac{qe}{Ce} = \text{lnke}\, qm - \frac{qe}{qm}$$

The slopes and intercepts of the plot ln(qe/Ce) vs qe can be used to determine the Elovich maximum adsorption capacity and Elovich constant if the adsorption follows the Elovich equation. The adsorption of copper on AC, ZnO, and ZnO/AC does not fit the Elovich isotherm, as can be seen from Figure 9 and Table 2, where the values of the regression coefficient R^2 were 0.251, 0.8393, and 0.3235 for AC, ZnO, and ZnO/AC, respectively. These values are higher than those for Langmuir and lower than Henry's and Freundlich

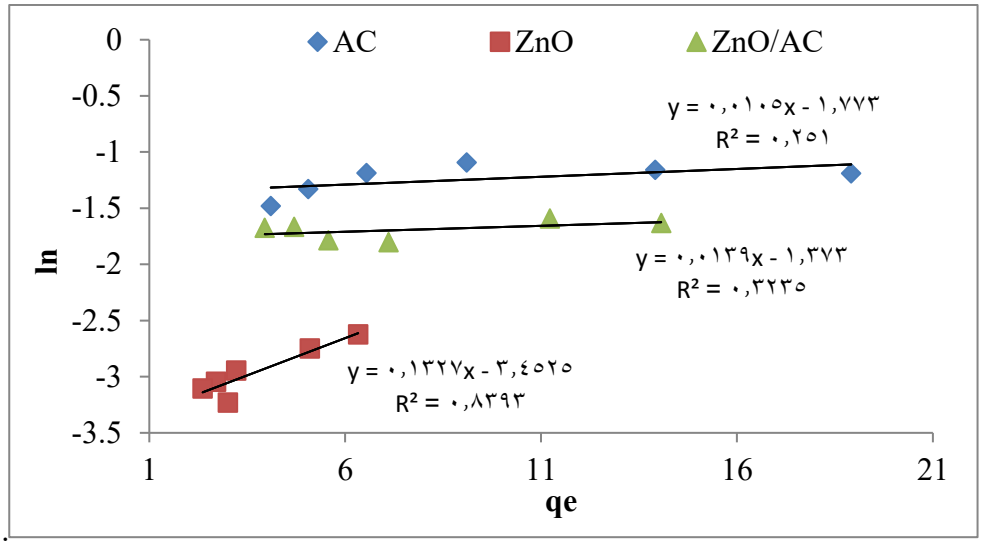

isotherms.

Fig. 9. Elovich adsorption isotherm.

Temkin Isotherm

The Temkin isotherm model assumes that the heat of adsorption (ΔH_{ads}) of all molecules in the layer declines linearly with increasing surface coverage and accounts for the impact of indirect adsorbate/adsorbate interactions on the adsorption process. Only an intermediate range of ion concentrations can be used with the Temkin isotherm.

$$qe = bT \ln kT \quad + bT \ \boldsymbol{lnCe}$$

lnCe is the linear form of the Temkin isotherm model, where T is the Temkin constant, which is correlated with the heat of sorption (J mol^{-1}), and T is the Temkin isotherm constant (Lg^{-1}). In order to verify that the adsorption of Eosin Yellow dye onto Cr_2O_3 nanoparticles is a result of chemisorption, Maryam and her collaborator used the Temkin isotherm model [16].

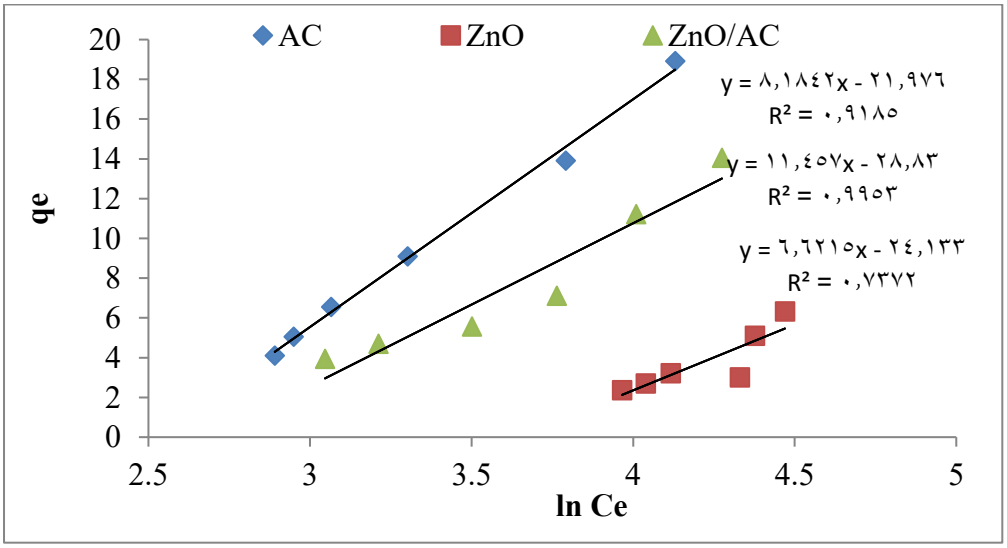

Fig. 10. Temkin adsorption isotherm.

Table 2: Isotherm constants of copper adsorption

Isotherm model	Adsorbent	Parameter	Value	R^2
Henry	AC	K_{HE}	0.323521	0.9839
	ZnO	K_{HE}	0.098896	0.769
	ZnO/AC	K_{HE}	0.205162	0.976
Langmuir	AC	q_m K_L	72.52 0.0035	0.2223
	ZnO	q_m K_L	5.814 0.00548	0.3132
	ZnO/AC	q_m K_L	119.755 0.00144	0.1203
Freundlich	AC	Kf nf	0.170519 0.863694	0.9733
	ZnO	Kf nf	0.003109 0.598936	0.7772
	ZnO/AC	Kf nf	0.155374 0.955096	0.9614
Temkin	AC	b_T K_T	11.45716 0.080752	0.9185
	ZnO	b_T K_T	6.621546 0.026131	0.7372
	ZnO/AC	b_T K_T	8.184178 0.068206	0.9953
Elovich	AC	q_m K_E	71.59 1.019266	0.251
	ZnO	q_m K_E	7.735 1.581	0.8393
	ZnO/AC	q_m K_E	94.832 1.018872	0.3235

Conculsion

The ability to successfully predict and interpret adsorption isotherms has a significant impact on the degree of accuracy that may be acquired from adsorption operations. Despite this, because linear regression analysis is widely applicable to a wide range of adsorption data, it has been widely utilized to assess the quality of fits and adsorption performance. Through the use of an adsorption technique, copper ions were effectively removed from aqueous solution using a sorbent composed of nanomaterials. Using the Langmuir, Freundlich, Temkin, Elovich, and Henry's isotherms, the equilibrium data were examined. The order in which to fit isotherms was shown by correlation coefficients: Henry's > Freundlich > Temkin > Elovich > Langmuir. Additionally, the pseudo-first order and pseudo-second order models

were used to investigate kinetic parameters. According to kinetic investigations, both models were followed in the adsorption of copper ions onto AC, ZnO, and ZnO/AC.

References

1. Jessica Briffa, Emmanuel Sinagra, Renald Blundell. Heavy metal pollution in the environment and their toxicological effects on humans. Heliyon. **2020**, 6(9), e04691.
2. Kosar Hikmat Hama Aziz, Fryad S. Mustafa, Khalid M. Omer, Sarkawt Hama, Rebaz Fayaq Hamarawf, and Kaiwan Othman Rahman. Heavy metal pollution in the aquatic environment: efficient and low-cost removal approaches to eliminate their toxicity: a review. RSC Adv. **2023**, 13(26), 17595–17610.
3. Yongming Liu, Haishuang Wang, Yuanyuan Cui and Nan Chen. Removal of Copper Ions from Wastewater: A Review. Int. J. Environ. Res. Public Health. **2023**, 20(5), 3885.
4. Fei Wu, Jing Wang, Chunwen Pu, Liang Qiao, and Chunmeng Jiang. Wilson's Disease: A Comprehensive Review of the Molecular Mechanisms. Int J Mol Sci. **2015**, 16(3), 6419–6431.
5. Grzegorz Izydorczyk, Katarzyna Mikula, Dawid Skrzypczak, Konstantinos Moustakas, Anna Witek-Krowiak, Katarzyna Chojnack. Potential environmental pollution from copper metallurgy and methods of management. Environmental Research. **2021**,197, 111050.
6. Taylor, A.A., Tsuji, J.S., Garry, M.R. et al. Critical Review of Exposure and Effects: Implications for Setting Regulatory Health Criteria for Ingested Copper. Environmental Management. **2020**, 65, 131–159.
7. Qasem, N.A.A., Mohammed, R.H. & Lawal, D.U. Removal of heavy metal ions from wastewater: a comprehensive and critical review. npj Clean Water. **2021**, 4, 36.
8. Niraj S. Topare , Vinayak S. Wadgaonkar. A review on application of low-cost adsorbents for heavy metals removal from wastewater. Materials Today. **2023**, 77(1), 8-18.
9. Rohit Kumar, Protima Rauwel, and Erwan Rauwel. Nanoadsorbants for the Removal of Heavy Metals from Contaminated Water: Current Scenario and Future Directions. Processes. **2021**, 9(8), 1379.
10. Rabia Baby, Mohd Zobir Hussein, Abdul Halim Abdullah, and Zulkarnain Zainal. Nanomaterials for the Treatment of Heavy Metal Contaminated Water. Polymers (Basel). **2022**, 14(3), 583.

11. Susy Prabawati , Priyagung Dhemi Widiakongko, Mohammad Ahsani Taqwim. Activated Charcoal from Coffee Dregs Waste as an Alternative Biosorbent of Cu(II) and Ag(I). Indonesian Journal of Chemistry. **2023**, 23(4),1120.
12. Alexandra Cristina Blaga, Alexandra Maria Tanasă, Ramona Cimpoesu, Ramona-Elena Tataru-Farmus, and Daniela Suteu. Biosorbents Based on Biopolymers from Natural Sources and Food Waste to Retain the Methylene Blue Dye from the Aqueous Medium. Polymers (Basel). **2022**, 14(13), 2728.
13. Zarifeh Raji, Ahasanul Karim, Antoine Karam, and Seddik Khalloufi. Adsorption of Heavy Metals: Mechanisms, Kinetics, and Applications of Various Adsorbents in Wastewater Remediation—A Review. Waste **2023**, 1(3), 775-805.
14. Eduardo Leiva, Camila Tapia, and Carolina Rodríguez. Highly Efficient Removal of Cu(II) Ions from Acidic Aqueous Solution Using ZnO Nanoparticles as Nano-Adsorbents. Water **2021**, 13(21), 2960.
15. Dar, R.A., Naikoo, G.A., Srivastava, A.K. et al. Performance of graphene-zinc oxide nanocomposite coated-glassy carbon electrode in the sensitive determination of para-nitrophenol. Sci Rep, **2022**, 12, 117.
16. Maryam Hassan Fadhel, Alaa Hasan Fahmi, Abdulqadier Hussien Al Khazraji. Synthesis of Different Nanoparticle Materials and Impregnated into Different Materials to Enhance the Eosin Yellow Dye Adsorption. Thesis , College of Education for Pure Science Department of Chemistry, University of Diyala, Iraq, **2022**.